Design and Analysis of DC-DC Converters with Artificial Intelligence Based MPPT Approaches for Grid Tied Hybrid PV-PEMFC System

B. Raja Sekhar Reddy[1,*], V. C. Veera Reddy[2] and M. Vijaya Kumar[1]

[1]*Department of EEE, J N T University, Ananthapuramu, Andhra Pradesh, India*
[2]*School of Engineering and Technology, SPMVV, Tiurpati, Andhra Pradesh, India*
E-mail: rajabayyapureddy@gmail.com
[*]*Corresponding Author*

Received 27 March 2022; Accepted 03 November 2022;
Publication 16 May 2023

Abstract

Renewable energy sources (RES) are inherently stochastic, require the deployment of an energy storage device to round off variations in power. A hybrid system consisting solar PV and PEMFC for grid-connected applications is proposed and analysed. For grid-tied applications, a radial basis function network (RBFN) type maximum power point tracking (MPPT) approach for PEM (Proton Exchange Membrane) fuel cells and a fuzzy logic controller (FLC) type MPPT approach for Photovoltaic system respectively is developed and analysed. In addition, a high step-up hybrid boost converter (HSHBC) for fuel cells has been designed, which provides a higher voltage gain than a conventional Boost converter. Developing a fuzzy logic controller for PV system at different solar irradiation levels and a RBFN based

Distributed Generation & Alternative Energy Journal, Vol. 38_4, 1307–1330.
doi: 10.13052/dgaej2156-3306.38410

MPPT technique for PEM Fuel Cell with different temperatures respectively to get the maximum power. The developed system is simulated using the Simulink/MATLAB platform to analyse it.

Keywords: Hybrid PV-PEMFC system, radial basis function network, high step-up hybrid DC-DC converter, conventional boost converter, PV system, PEMFC, MPPT.

1 Introduction

Because of the growth in load demand on the power system , the use of fossil fuels such as coal, gas and other fuels has increased fast, causing major issues and environmental repercussions [1–3]. Because fossil fuels are non-renewable, they may run out in the next several decades [4–7]. As a result, multiple energy sources must be integrated together using power electronic converters to produce a hybrid system. A MPP Tracking approach is required for tracking the maximum power from high penetration renewable sources [8]. Because of their abundance in nature, several academics have concentrated their study on hybrid PV and wind energy systems [9]. Solar irradiation and wind speed have an impact on PV and wind energy sources, respectively [10]. Solar energy, which is available vastly, and the high energy density of fuel cells, a right amalgam of PV and fuel cell sources is an acceptable solution for the HRES [11]. A PV system's maximum power point (MPP) changes with irradiance and temperature. The MPP of a Fuel Cell, on the other hand, is affected by variations in membrane water content and cell temperature [12]. For harvesting maximum power from hybrid PV and PEM fuel cell sources, a large range of maximum power tracking techniques are available in the literature. Available maximum power tracking techniques [13–15] has number of benefits and drawbacks.

The electrolyte component utilized in fuel cells classifies them into several categories. PEMFC is the most often used kind in electrical applications due to its less noise, compact size and large power density [16].

To enhance the PV and PEMFC systems output voltages are fed through DC-DC converters. Through an inverter, the DC link's output is fed into the grid. The basic topology of Hybrid solar PV-PEMFC system is depicted in Figure 1.

In Figure 2, the Three Phase Grid Tied Hybrid PV-PEMFC system is depicted. The input power is provided by a solar PV and PEMFC system. To enhance the solar PV and PEMFC system output voltages a DC-DC

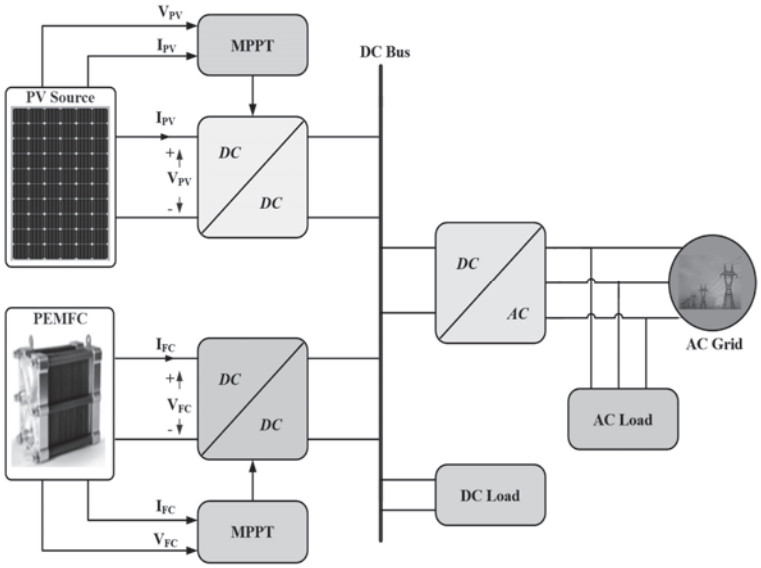

Figure 1 Hybrid PV-PEMFC system.

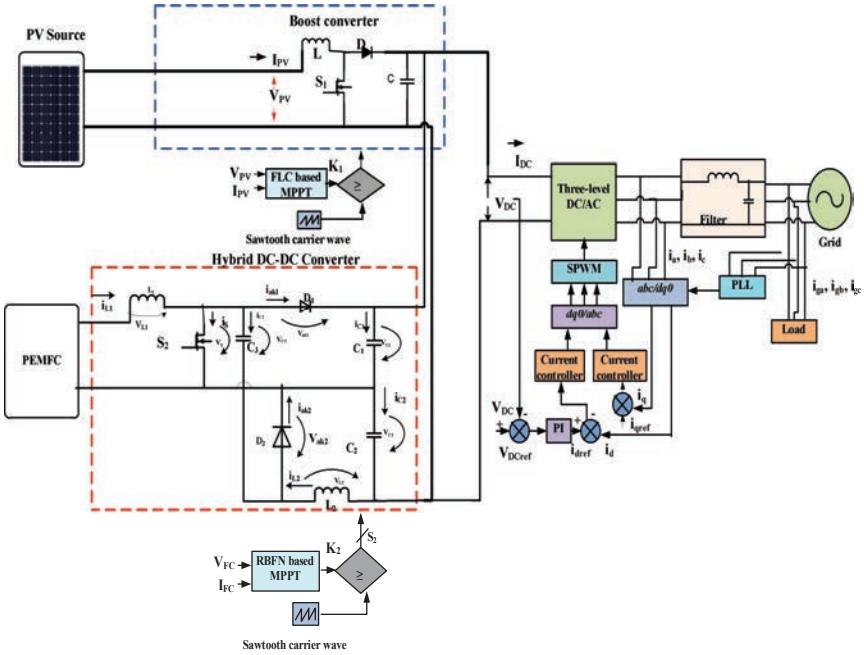

Figure 2 The proposed grid-connected hybrid solar PV-PEMFC system.

Converter and a HSHBC is used. The HSHBC uses a single switch which increases the efficiency of PEMFC systems. FLC based and RBFN based MPP Tracking Techniques for PV system and PEMFC system are developed. This generated output voltage is fed into AC grid of rating 2 kW, 230 V, 50 Hz.

2 Hybrid System

2.1 Photovoltaic System

The single model diode Photovoltaic cell equivalent circuit is depicted in Figure 3. The basic I_{PV}–V_{PV} characteristics of PV panels are used to develop the mathematical modelling of the Photovoltaic system. Equations (1) and (2) respectively, are the fundamental equations of PV system [17, 18].

$$V_{\mathrm{PV}} = \frac{\eta \mathrm{KT}}{q} \ln\left(\frac{I_{\mathrm{Ph}}}{I_{\mathrm{PV}}} + 1\right) \tag{1}$$

$$I_{\mathrm{PV}} = I_{\mathrm{ph}} - I_D\left[\exp\left(\frac{q(V_{\mathrm{PV}} + R_{Se} I_{\mathrm{PV}})}{\eta \mathrm{KT}}\right) - 1\right] - \frac{V_{\mathrm{PV}} + R_S I_{\mathrm{PV}}}{R_{\mathrm{Sh}}} \tag{2}$$

Where,

V_{PVV}: Output voltage of Photovoltaic panel (Volts)
I_{PVI}: Output current of Photovoltaic panel(Amps)
I_{PhP}: Phase current of PV cell
I_{DS}: Diode – saturation current
Q_E: Electron charge of 1.698* 10^{-19} C
η: ideality factor
K_B: Boltzmann constant – 1.38*10 $^{-23}$ J/K
R_{Se} and R_{Sh}: Cell's series and parallel resistances
T_{PV}: PV system's temperature.

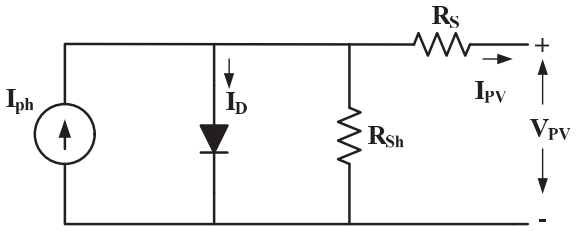

Figure 3 PV cell equivalent circuit.

Table 1 The proposed 950W BP solar SX 3190 PV system parameters

Description	Rating
Number of PV cells connected in parallel	5
Irradiation	600–1000 W/m^2
Temperature	25°C
Open circuit voltage	30.6 V
Short circuit current	8.51 A
Maximum power	950 W
Maximum voltage	24.3 V
Maximum current	7.829 A

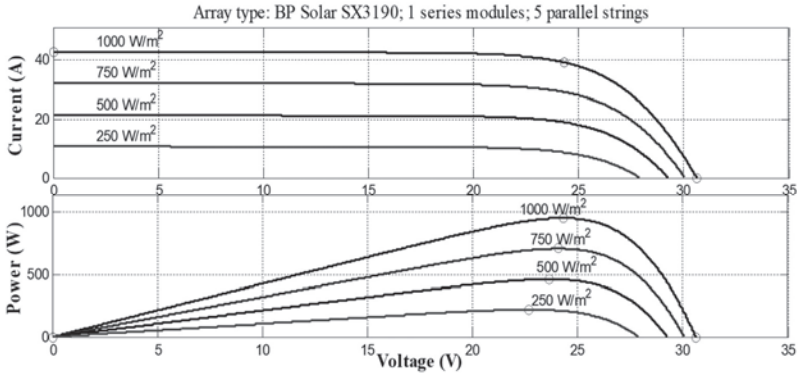

Figure 4 Characteristics of PV cell at different irradiation conditions.

The 950W BP Solar SX3190 PV module is used to implement a hybrid renewable energy system, and design specifications are provided in the Table 1. Figure 4 shows the I-V and P-V characteristics of the Photovoltaic module on the basis of solar irradiation availability. The PV system output power is clearly noticed to be dependent on the solar irradiation availability and temperature.

2.2 PEMFC

The schematic arrangement of the PEMFC is shown in Figure 5 [19, 20]. The following is the operational principle:

$$\begin{cases} 2H_2 \rightarrow 4H^+ + 4e^- \\ O_2 + 4H^+ + e^- \rightarrow 2H_2O \\ 2H_2 + O_2 \rightarrow 2H_2O + \text{energy} \end{cases} \tag{3}$$

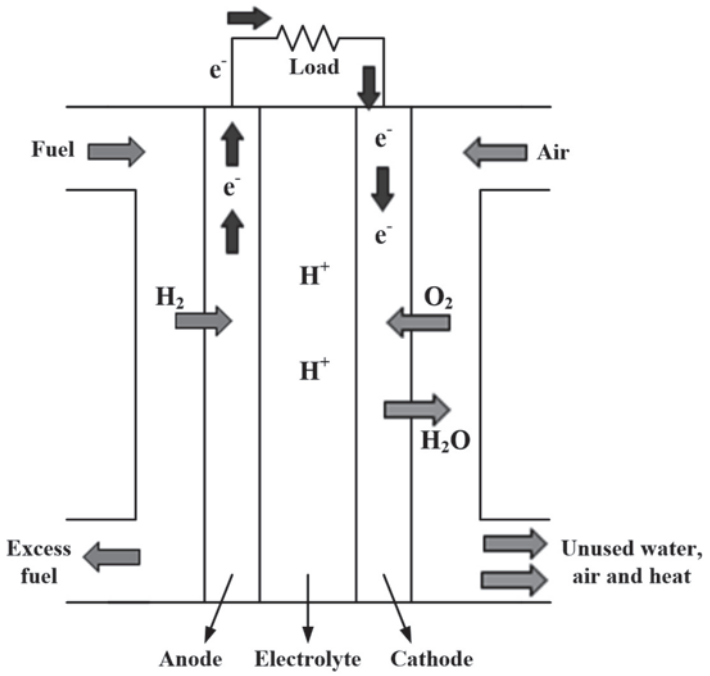

Figure 5 Schematic layout fuel cell.

Figure 6 depicts the electrical representation of a PEMFC.
The Equation (4) is used to calculate the PEMFC stack terminal voltage.

$$\mathrm{V_S} = \mathrm{nV_{PEM}} \tag{4}$$

Where,

n: Series connected PEM Fuel Cell
$\mathrm{V_{PEM}}$: Single PEMFC cell output voltage [21].

$$\mathrm{V_{PEM}} = \mathrm{E_{Nerst}} - \mathrm{V_{OHm}} - \mathrm{V_{ACt}} - \mathrm{V_{CoN}} \tag{5}$$

Where,

$\mathrm{T_{Nerst}}$: Thermodynamic open circuit voltage

$$\mathrm{T_{Nerst}} = 1.229 - 8.5\mathrm{e}^{-4}(\mathrm{T_{PEM}} - 298.15) + 4.308\mathrm{e}^{-5}[\ln(\mathrm{P_{HG2}}) + 0.5\ln(\mathrm{P_{OG2}})] \tag{6}$$

$\mathrm{V_{OHm}}$: Activation overvoltage

$$\mathrm{V_{OHm}} = \mathrm{R_{FC}} \cdot \mathrm{I_{FC}} \tag{7}$$

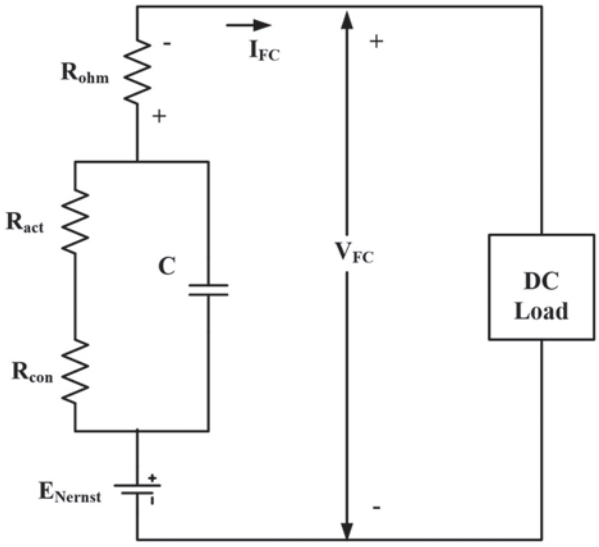

Figure 6 Electrical model of PEMFC.

V_{AC}: Activation overvoltage

$$V_{ACt} = T_{Fc}(x + y\ln(I_{FC})) \tag{8}$$

V_{Con}: Concentration voltage.

$$V_{CoN} = -0.016\ln\left(1 - \frac{I_{FC}}{25}\right) \tag{9}$$

Where,

P_{HG2}: Partial pressure of hydrogen gas
P_{OG2}: Partial pressure of oxygen gas
T_{PEM}: PEM Fuel Cell temperature
I_{PEM}: PEM Fuel Cell current
x and y: constants.

Figure 7 shows the PEM Fuel Cell I-V and P-V characteristics. The specifications of parameter are enumerated in Table 2.

3 Design of DC-DC Boost Converters

Two independent DC-DC converters are employed in the hybrid solar PV and PEMFC system to maintain voltage at the DC link. In the solar PV system,

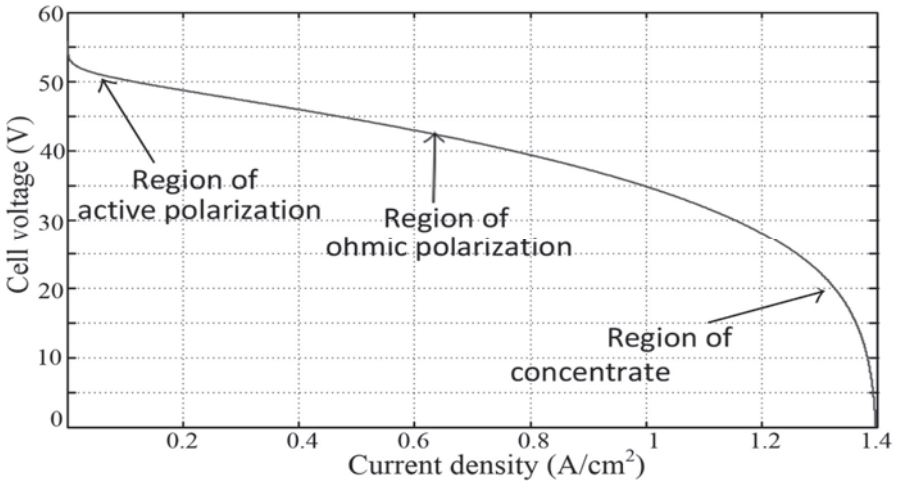

Figure 7 V-I characteristics of PEMFC.

Table 2 1.26 kW PEM fuel cell parameter specifications

Description	Value
Number of Cells	42
Maximum Power	1260 W
Maximum Voltage	24.23 V
Maximum Current	52 A
Hydrogen Partial Pressure	1.5 bar
Oxygen Partial Pressure	1 bar
Nominal Fuel Flow Rate	417.3 lpm
Nominal Air Flow Rate	2400 lpm

a conventional DC-DC boost converter is utilised, but in the PEMFC system, HSHBC is utilised.

3.1 Conventional Boost Converter

The conventional DC-DC boost converter, as illustrated in Figure 8, has a higher conversion efficiency, a simpler construction with fewer converter components, and its convert low source voltage to required value by increasing the duty cycle at a higher switching frequency rate [22].

As shown in Figure 8, the DC-DC converter has a switch, a Inductor, a diode, and a capacitor.

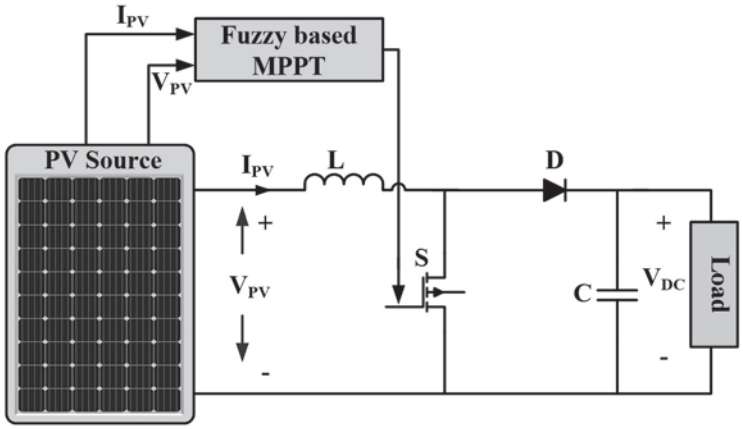

Figure 8 Equivalent circuit of conventional boost converter with PV system.

The diode reaches reverse bias mode when the switch is turned on. In this scenario, the supply voltage is utilised to charge inductor. The voltage across the inductor L is

$$V_L = V_{PV} \tag{10}$$

The diode is in forward bias when the switch S is off. The inductor voltage may be calculated using the following equation:

$$V_L = V_{PV} - V_{DC} \tag{11}$$

Apply Volt-second balance condition on inductor *L*

$$V_{PVS} \cdot \mathrm{K}_1 + (V_{PVS} - V_{Dc}) \cdot (1 - \mathrm{K}_1) = 0 \tag{12}$$

Based on Equation (12),

$$\text{The voltage gain } M_1 = \frac{V_{DC}}{V_{PV}} = \frac{1}{1 - K_1} \tag{13}$$

By using the following equations, The inductor *L* and capacitor *C* is

$$L = \frac{V_{\mathrm{FC}} K_1 T_S}{\Delta I_L} \tag{14}$$

$$C = \frac{I_{\mathrm{DC}} K_1 T_S}{\Delta V_{\mathrm{DC}}} \tag{15}$$

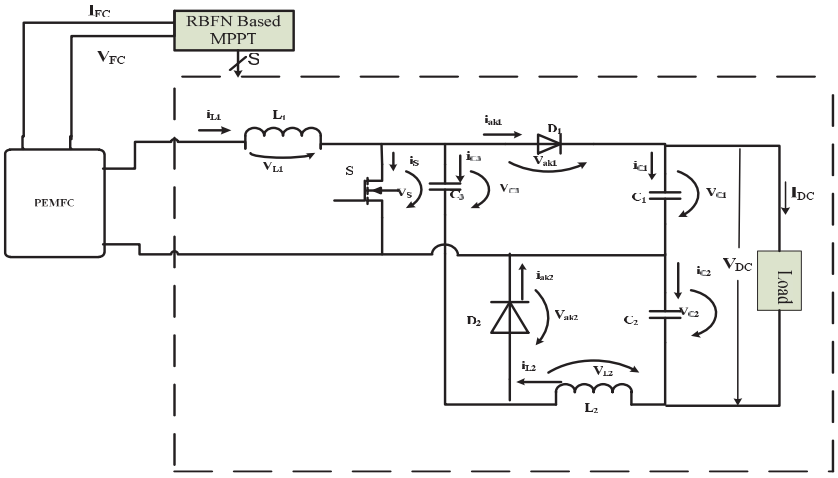

Figure 9 High step-up hybrid Boost converter.

3.2 High Step-up Hybrid DC-DC Converter (HSHBC)

By combining the input stages of boost and cuk converters, the HSHBC is suggested and is depicted in Figure 9. The proposed HSHBC topology is analysed in continuous conduction mode by assumption that all components are assumed to be ideal [23, 24]. As a result of this, the three operational modes which are given below can be defined:

(1) Operating mode a [$t_1 - t_2$]: The operating mode (a) from [$t_1 - t_2$] is active when the power switch is turned on. While both inductors are charging, capacitor C_3 is draining. The negative voltages V_{c1} and V_{c3} block diodes both diodes.

(2) Operating mode b [$t_2 - t_3$]: In this mode the power switch is switched off, the operation effective. This working mode arises because the voltage across capacitor C_3 is lower than the voltage across capacitor C_1. During this time, the energy of inductors L_1 and L_2 is reducing, while capacitor C_3 is being charged. The diode D_1 will remain turned off when the diode D_2 is turned on.

(3) Operating mode c [$t_3 - t_4$]: This working mode will be effective when the power switch is turned off and the voltage across capacitor C_1 is equal to or less than the voltage across capacitor C_3. The capacitors C_1 and C_3 are charged by the current passing via the inductor L_1. Both inductors are in the process of discharging. The diodes have both been turned on.

The static voltage gain (G) in CCM is as follows

$$\frac{V_0}{V_i} = \frac{1+\delta}{1-\delta} \tag{16}$$

The inductance value of L_1 will be determined in proportion to the PV output current at MPP to ensure a low current ripple i_1. When the power switch is ON, the inductor current may be expressed as (17) by using inductor voltage v_{L_1}.

Considering $\Delta t_{on} = \delta T$ in (17) and $\Delta i_{L1} = i_{L1}(t) - i_{L1}(t_0)$.

Where V_i: maximum PV output voltage at MPP.

The inductor L_1 be determined by (18).

$$i_{L_1}(t) = \frac{v_{L_1}}{L}\Delta t_{on} + i_{L_1}(t_o) \tag{17}$$

$$L_1 = \frac{V_i \delta T}{\Delta i_{L_1}} \tag{18}$$

By applying the same procedure, the inductor L2 value can be attained.

The power switch S OFF time $\Delta t_{off} = (1-\delta)T$.

The inductor L_2 can be defined by

$$L_2 = \frac{V_{C_2}(1-\delta)T}{\Delta i_{L_2}} \tag{19}$$

A similar procedure can be used for the capacitors C1 and C3. This approach, like the inductors (18) and (19), considers the discharge times $\Delta t1$ and $\Delta t2$ with relation to duty cycle when determining capacitors C1 and C3. This approach, however, is only valid in steady-state operation. To assure dynamic behaviour, the times t_1 and t_2 are settling periods of the currents in inductors L_1 and L_2, respectively, and load power P_0 in (20) and (21).

$$C_1 = \frac{1}{\Delta V_{C_1}}\frac{P_0}{V_o}\Delta t_1 \tag{20}$$

$$C_3 = \frac{1}{\Delta V_{C_3}}\frac{P_0}{V_o}\Delta t_2 \tag{21}$$

When the change in charge of the capacitor C2 is proportional to the change in current in the inductor $L2\Delta i_{L_2}$, the value of capacitor C2 may be calculated. Thus, from (22) and (23) the capacitor C2 can be obtained.

$$C_2 = \frac{\Delta Q}{\Delta V_{C_2}} \tag{22}$$

$$\Delta Q = \frac{\frac{T}{2}\frac{\Delta i_{L_2}}{2}}{2} \tag{23}$$

$$C_2 = \frac{T\Delta i_{L_2}}{8\Delta V_{C_2}} \tag{24}$$

4 MPPT Controllers

4.1 Fuzzy Logic Controller MPPT Technique for Photovoltaic System

Fuzzy Logic Controller is a rule-based method that uses membership functions to operate. Fuzzy Logic Controller offers the advantages of being simple to use, quick to respond, and have a user-friendly interface [25]. Figure 10 shows the FLC architecture, which includes fuzzification, inference engine, rule base, and defuzzification and the FLC has two input variables: error (F) and change in error (ΔF), with change in duty cycle (D) as the output variable [26, 27]. The error E is defined as follows

$$\mathrm{F(n)} = \frac{\mathrm{P_{SPV}(n)} - \mathrm{P_{SPV}(n-1)}}{\mathrm{V_{SPV}(n)} - \mathrm{V_{SPV}(n-1)}} \tag{25}$$

The change in error is

$$\Delta\mathrm{F} = \mathrm{F(n)} - \mathrm{F(n-1)} \tag{26}$$

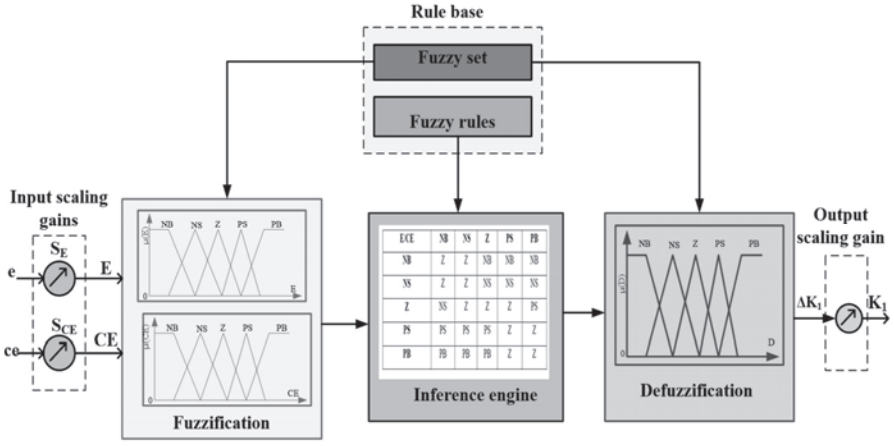

Figure 10 Fuzzy logic controller structure.

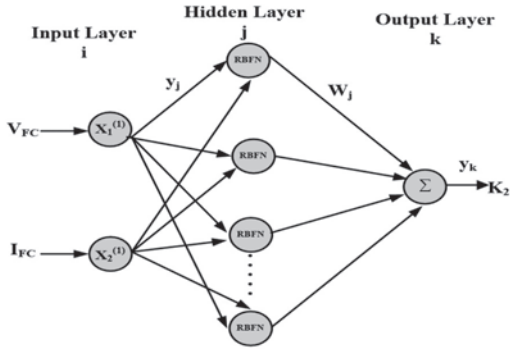

Figure 11 RBFN architecture.

Where,

$P_{SPV}(n)$: Solar PV system Instant Power
$V_{SPV}(n)$: Solar PV system Voltage

Fuzzification stage: The input variables are converted as linguistic functions. The rules in the rule base are used to change the inference engine's language functions. The membership functions are used to turn the linguistic parameters into a numerical number during the defuzzification step [28, 29]. Mamdani's approach is used to create the membership functions.

4.2 RBFN Based MPPT Technique for PEM Fuel Cell

The RBFN model is a supervised and unsupervised learning feed-forward neural network. In most cases, RBFN comprises three layers as follows; (i) Input , (ii) hidden and (iii) output as depicted in Figure 11. The training approach for the RBFN is separated into two sections. In the unsupervised training technique, radial basis functions are used to control the input parameters. After that, the weights are learned using supervised training, which is similar to the backpropagation training method. The V and I from the PEM Fuel Cell are inputs to the RBFN Controller and control signal as output that is supplied to the HSHBC to boost the output voltage.

The RBFN input layer has two neurons.

The data is transferred to the hidden layer.

The net input and net output of the input layer are as follows:

$$x_i^{(\mathbf{1})}(n) = \mathrm{net}_i^{(1)} \tag{27}$$

$$y_i^{(\mathbf{1})}(n) = f_i^{(\mathbf{1})}[\mathrm{net}_i^{(\mathbf{1})}(n)] = \mathrm{net}_i^{(\mathbf{1})}(n), i = 1, 2 \tag{28}$$

Where,

$x_i^{(\mathbf{1})}$: input layer

$y_i^{(\mathbf{1})}$: Hidden layer

$\mathrm{net}_i^{(\mathbf{1})}$: Input layer's sum.

A Gaussian function is executed by each node in the hidden layer.

$$net_j^{(\mathbf{2})}(n) = -(X - M_j)^T \sum_j (X - M_j) \tag{29}$$

$$y_j^{(\mathbf{2})}(n) = f_j^{(\mathbf{2})}[\mathrm{net}_j^{(\mathbf{2})}(n)]\exp[\mathrm{net}_j^{(\mathbf{2})}(n)],\ j = 1, 2, \ldots \tag{30}$$

M_j and $\sum_{\mathbf{j}}$ are the Gaussian function's mean and standard deviation respectively. The linear control signal (K_2) is generated by the output layer, which contains a single node t.

$$\mathrm{net}_t^{(3)} = \sum_j w_j y_j^{(\mathbf{2})} \tag{31}$$

$$y_t^{(\mathbf{3})} = f_t^{(\mathbf{3})}[\mathrm{net}_t^{(\mathbf{3})}(n)] = \mathrm{net}_t^{(\mathbf{3})}(n) \tag{32}$$

where w_j: Between the output and the hidden layer, there is a weight matrix.

After Radial Basis Function Network has been initialised, the system is trained using a supervised training technique. The backpropagation method is analogous to this training procedure. It is important to use training patterns to tune the RBFN's parameters. The supervised training algorithm determines and updates the error of each layer in RBFN. The system error E is

$$E = \sum \frac{1}{2}(V_{\mathrm{DC}} - V_{\mathrm{MPP}}) \tag{33}$$

Where,

V_{DC}: Pre-defined or Reference output voltage

V_{MPP}: Obtained or Actual output voltage.

The RBFN MPPT technique for PEMFC systems is depicted in Figure 12. The proposed RBFN controller Input variables are temperature, current and output variable is duty cycle is depicted in Figure 13 and the optimal parameters of proposed RBFN controller are mentioned in Table 3.

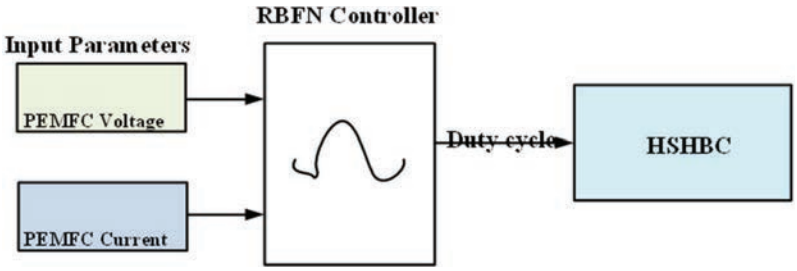

Figure 12 RBFN controller for PEMFC.

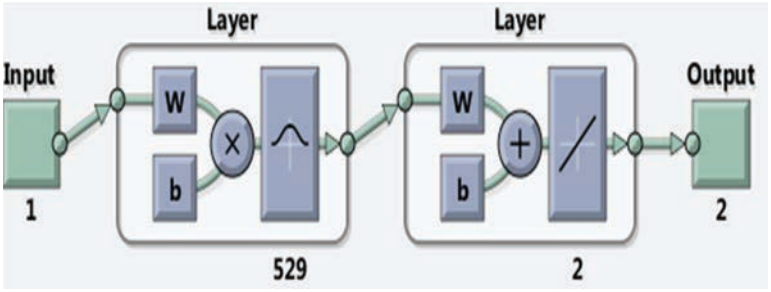

Figure 13 Proposed RBFN based MPPT architecture.

Table 3 Proposed RBFN architecture optimal parameters

Parameter Description	Value
Input variables	V_{FC} & I_{FC}
Output variable	Duty Cycle (D)
Spread factor	0.01
Hidden neurons maximum limit	529

5 Results and Discussions

A Matlab/Simulink model is created for a grid-connected hybrid renewable energy system with a load of 2000 watts active power and 800 VAR reactive power with an AC grid rating of 230 V, 50 Hz. The three phase Inverter receives power from the common DC connection. When the I_Q and V_{DC} generated are compared to the reference values, the error is passed to the PI controller, which creates the firing angle.

The proposed system's solar irradiation availability is calculated as follows and depicted in Figure 14 G = 800w/m^2 for 0 sec to 0.3 sec (20% shading effect), G = 600 w/m^2 for 0.3 sec to 0.6 sec (40% shading effect),

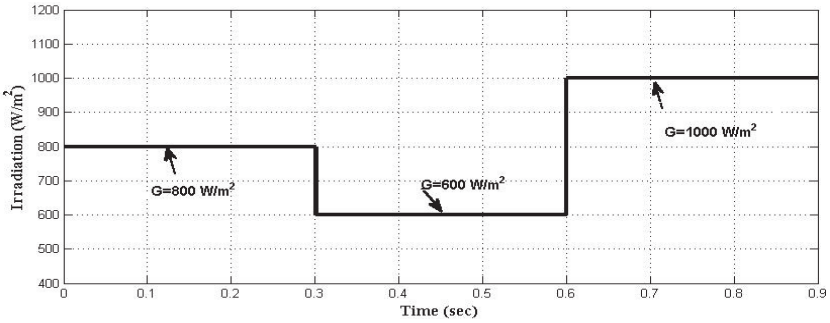

Figure 14 Solar irradiation levels.

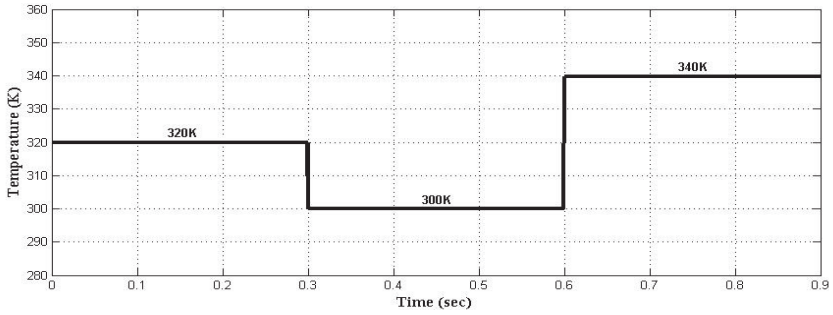

Figure 15 PEMFC system temperature variations.

and G = 1000 w/m^2 for 0.6 sec to 0.9 sec (0 percent shading effect). PEMFC temperatures are 320 K for 0 sec to 0.3 sec, 300 K for 0.3 sec to 0.6 sec, and 340 K for 0.6 sec to 0.9 sec, as illustrated in Figure 15.

The PV system and PEMFC system voltage, current and power output waveforms at considered radiations and temperatures are shown in Figures 16 and 17 respectively. The voltage and current waveforms of load, inverter and grid are shown in Figures 18, 19 and 20 respectively.

Figure 21 depicts the active power profile of the load, inverter, and grid, whereas Figure 22 depicts the reactive power profile of the load, inverter, and grid. The hybrid system and grid meet the load demand of 2000 Watts active power and depicted in Figure 21. The load requirement is satisfied by both hybrid and grid sources for various time periods: 1500 Watts and 400 Watts from 0 to 0.3 sec, 1090 Watts and 900 Watts from 0.3 to 0.6 sec, and 1880 Watts and 110 Watts from 0.6 to 0.9 sec, respectively. The reactive power load of 800 VAR is met by the both systems and depicted in Figure 22. The active power profile and reactive power profiles are depicted in Table 4.

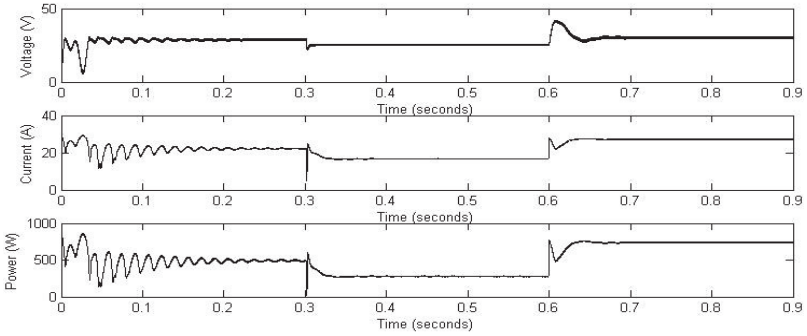

Figure 16 Photovoltaic panel Voltage, current, and power at the output.

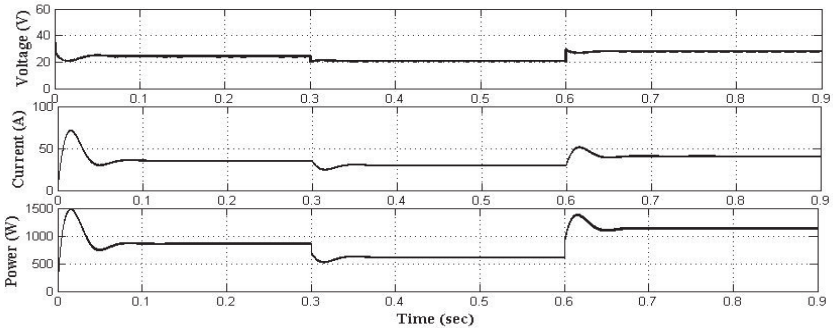

Figure 17 PEM Fuel Cell voltage, current and power at the output.

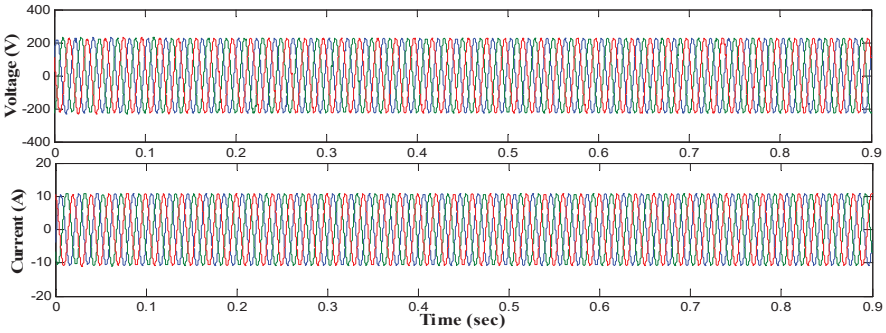

Figure 18 Load current and voltage waveforms.

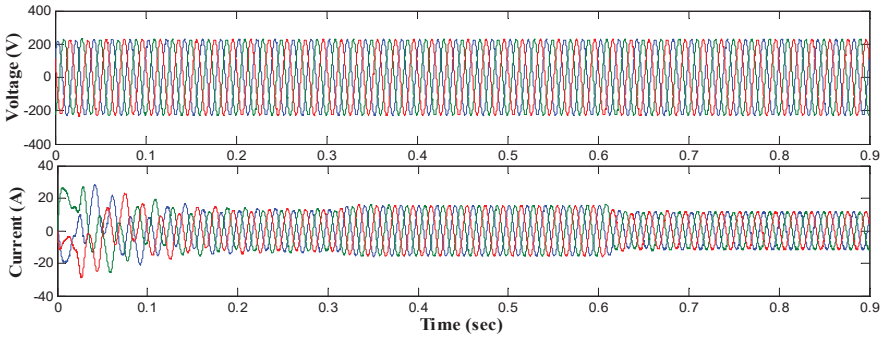

Figure 19 Current and voltage waveforms of inverter.

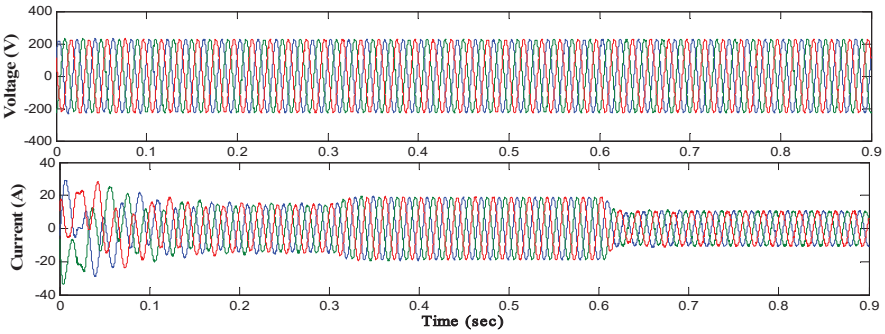

Figure 20 Current and voltage waveforms of grid.

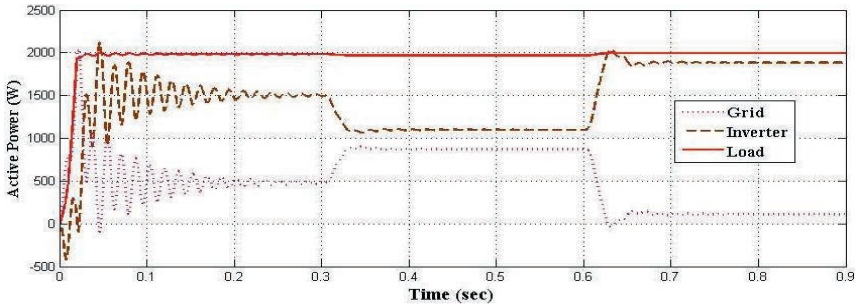

Figure 21 Active power profile.

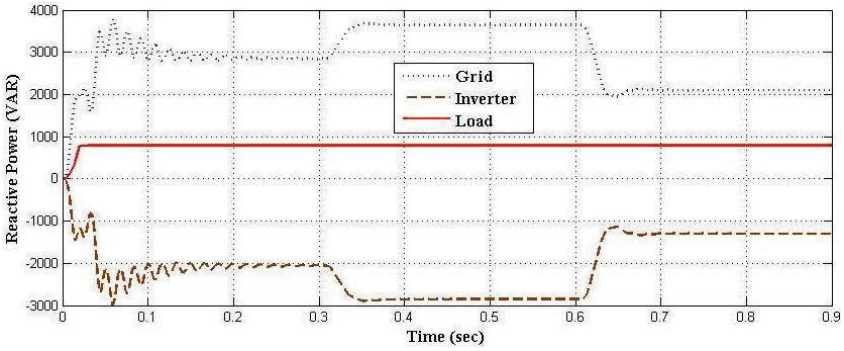

Figure 22 Reactive power profile.

Table 4 Active and reactive power profiles

Parameter	Time Period (Sec)	Load Output (Watts)	Inverter Output (Watts)	Grid Output (Watts)
Active Power	0 to 0.3	1990	1500	490
	0.3 to 0.6	1990	1090	900
	0.6 to 0.9	1990	1880	110
Reactive Power	0 to 0.3	795	−2135	2930
	0.3 to 0.6	795	−2935	3730
	0.6 to 0.9	795	−1255	2050

6 Conclusion

The contribution of this article could be summarized as follows: (1) proposing and implementing a three-phase grid tied hybrid PV and PEMFC system (2) Developing a fuzzy logic controller and a new RBFN based MPP Tracking technique for PV system at different solar irradiation levels and PEMFC system with different temperatures respectively to extract the maximum power. (3) A hybrid boost converter by integration of a Boost and Cuk conerters, using only one controlled switch is designed for PEMFC system to provide high voltage gain and conventional DC-DC converter for PV system. (4) A detailed simulation results are presented and verified. (5) The future work includes experimental verification of the proposed hybrid PV-PEMFC system.

References

[1] K. Kumar, N. Ramesh Babu, and K. R. Prabhu, "Design and analysis of an integrated Cuk-SEPIC converter with MPPT for standalone wind/PV hybrid system," Int. J. Renew. Energy Res., vol. 7, no. 1, pp. 96–106, 2017.

[2] G. Wu, X. Ruan, and Z. Ye, "Nonisolated high step-up DC–DC converters adopting switched-capacitor cell," IEEE Trans. Ind. Electron., vol. 62, no. 1, pp. 383–393, Jan. 2015.

[3] S. Saravanan and N. Ramesh Babu, "Modified high step-up coupled inductor-based DC-DC converter for PV applications," Gazi Univ. J. Sci., vol. 29, no. 4, pp. 981–986, 2016.

[4] S. Saravanan and N. Ramesh Babu, "RBFN based MPPT algorithm for PV system with high step up converter," Energy Convers. Manage., vol. 122, pp. 239–251, Aug. 2016.

[5] T.-J. Liang, J.-H. Lee, S.-M. Chen, J.-F. Chen, and L.-S. Yang, "Novel isolated high-step-up DC–DC converter with voltage lift," IEEE Trans. Ind. Electron., vol. 60, no. 4, pp. 1483–1491, Apr. 2013.

[6] M. Sitbon, S. Schacham, T. Suntio, and A. Kuperman, "Improved adaptive input voltage control of a solar array interfacing current mode controlled boost power stage," Energy Convers. Manage., vol. 98, pp. 369–375, Jul. 2015.

[7] M. E. Lotfy, T. Senjyu, M. A. Farahat, A. F. Abdel-Gawad, and A. Yona, "Enhancement of a small power system performance using multi-objective optimization," IEEE Access, vol. 5, pp. 6212–6224, 2017

[8] Rajkumar RK, Ramachandaramurthy VK, Yong BL, Chia DB, 'Techno-economical optimization of hybrid pv/wind/battery system using Neuro-Fuzzy', Energy, 36(8):5148–53, Aug 2011.

[9] Arul PG, Ramachandaramurthy VK, Rajkumar RK, 'Control strategies for a hybrid renewable energy system: A review', Renewable and Sustainable Energy Reviews, 42:597–608, Feb 2015.

[10] Behravesh V, Keypour R, Foroud AA, 'Stochastic analysis of solar and wind hybrid rooftop generation systems and their impact on voltage behavior in low voltage distribution systems', Solar Energy, 166: 317–33, May 2018.

[11] Basaran K, Cetin NS, Borekci S, 'Energy management for on-grid and off-grid wind/PV and battery hybrid systems', IET Renewable Power Generation, 11(5):642–9, Oct 2016.

[12] Thounthong P, Chunkag V, Sethakul P, Sikkabut S, Pierfederici S, Davat B, 'Energy management of fuel cell/solar cell/supercapacitor hybrid power source', Journal of power sources, 196(1):313–24, Jan 2011.

[13] Kamalapathi, K., Srinivasan Rao Nayak, P., and Kumar Tyagi, V. (2021). Analysis of Dual Input Buck-Boost Converter for Solar PV Integration with Wireless Electric Vehicle Charger. *Distributed Generation & Alternative Energy Journal*, *37*(1), 73–102.

[14] Kumar K, Babu NR, Prabhu KR, 'Design and Analysis of RBFN-Based Single MPPT Controller for Hybrid Solar and Wind Energy System', IEEE Access, 5:15308–17, 2017.

[15] S. Saravanan and N. Ramesh Babu, "Maximum power point tracking algorithms for photovoltaic system—A review," Renew. Sustain. Energy Rev., vol. 57, pp. 192–204, May 2016.

[16] Mebarki N, Rekioua T, Mokrani Z, Rekioua D, Bacha S, 'PEM fuel cell/battery storage system supplying electric vehicle', International Journal of Hydrogen Energy, 41(45):20993–1005, Dec 2016.

[17] Mebarki N, Rekioua T, Mokrani Z, Rekioua D, Bacha S, 'PEM fuel cell/battery storage system supplying electric vehicle', International Journal of Hydrogen Energy, 41(45):20993–1005, Dec 2016.

[18] C.-M. Hong and C.-H. Chen, "Intelligent control of a grid-connected windphotovoltaic hybrid power systems," Int. J. Elect. Power Energy Syst., vol. 55, pp. 554–561, Feb. 2014.

[19] F. Baghdadi, K. Mohammedi, S. Diaf, and O. Behar, "Feasibility study and energy conversion analysis of stand-alone hybrid renewable energy system," Energy Convers. Manage., vol. 105, pp. 471–479, Nov. 2015.

[20] Park JD, Ren Z, 'Hysteresis based maximum power point tracking energy harvesting system for microbial fuel cells', Journal of power sources, May 2012.

[21] Tirumalasetti, M. B., Manthati, U. B., Srinivas, P., and Arunkumar, C. R. (2022). A Novel Predictive Control Scheme for Interleaved Buck Converter in Low Power Applications. *Distributed Generation & Alternative Energy Journal*, *37*(3), 609–630. https://doi.org/10.13052/dgaej2156-3306.37311

Sekhar V, 'Modified fuzzy logic based control strategy for grid connected wind energy conversion system', Journal of Green Engineering, Oct 2016.

[22] Harrag A, Messalti S, 'How fuzzy logic can improve PEM fuel cell MPPT performances?' International journal of Hydrogen energy, Jan 2018.

[23] Kiruthiga K, Dyaneswaran A, Kavitha B, Prakash RA, 'Grid connected hybrid fuel cell- PO based MPPT for partially shaded solar Pv system', Int J P2P new trends technol, Apr 2014.
[24] Benyahia N, Denoun H, Zaouia M, Rekioua T, Benamrouche N, 'Power system simulation of fuel cell and super capacitor based electric vehicle using an interleaving technique', International journal of Hydrogen energy, Dec 2015.
[25] Allaoua B, Draoui B, Belatrache D, 'Study of the energy performance of a PEM fuel cell vehicle', International journal of Renewable energy research, Sep 2017.
[26] Gong W, Cai Z, 'Accelerating parameter identification of proton exchange membrane fuel cell model with ranking-based differential evolution Energy', Sep 2013.
[27] Tiwari R, Babu NR, 'Recent development of control strategies for wind energy conversion systems', Renewable and sustainable energy reviews, Dec 2016.
[28] Chakrapani, B. C. Arunkumar, C. R. Srinivas, P. and Manthati, U. B. (2022). Minimization of Circulating Currents in Parallel DC-DC Boost Converter Using Non-Linear Droop Control for Battery Energy Storage System. *Distributed Generation & Alternative Energy Journal*, *37*(3), 819–844.
[29] Praveen Kumar, T. Subrahmanyam, and Sydulu, M. Power Management System of a Particle Swarm Optimization Controlled Grid Integrated Hybrid PV/WIND/FC/Battery Distributed Generation System. *Distributed Generation & Alternative Energy Journal*, *36*(2), 141–168.
[30] Li Sun, Yuhui Jin, Lei Pan, Jiong Shen, Kwang Y. Lee, "Efficiency analysis and control of a grid-connected PEM fuel cell in distributed generation", Energy Conversion and Management, Volume 195, 2019, Pages 587–596, ISSN 0196-8904,

Biographies

B. Raja Sekhar Reddy, Received his B.Tech degree and M.E degree in Electrical and Electronics Engineering. He is currently a PhD Scholar in JNTUA, Electrical and Electronics Engineering, and his area of interests includes Renewable energy source, DC-DC Converters and Artificial Intelligence.

V. C. Veera Reddy received his B.Tech, M.Tech, and PhD degrees in Electrical and Electronics Engineering. He is worked as a professor at S.V University, Tirupathi. Presently, he is working as Professor Department of Electrical & Electronics Engineering, School of Engg. & Tech, Sr Padmavathi Mahila Vswavdyalayam, Thirupathi and his area of interests include power systems and renewable energy sources.

M. Vijaya Kumar, graduated from NBKR Institute of Science and Technology, Vidyanagar, A.P, India in 1988. He obtained M.Tech degree from Regional Engineering College, Warangal, India in 1990. He received Doctoral degree from JNT University, Hyderabad, India in 2000. He is currently working as a professor in EEE, JNTUA, Ananthapuramu. His areas of interests include Electrical Machines, Electrical Drives and Power Electronics.